Advanced Powder Technology 32 (2021) 2004–2019

Contents lists available at ScienceDirect

Advanced Powder Technology

journal homepage: www.elsevier.com/locate/apt

Original Research Paper

Thermal behavior and energy storage of a suspension of nano-encapsulated phase change materials in an enclosure

Mehdi Ghalambaz [a,b,*], S.A.M. Mehryan [c], Kasra Ayoubi Ayoubloo [d], Ahmad Hajjar [e], Mohammad S. Islam [f], Obai Younis [g,h], Abdelraheem M. Aly [i,j]

[a] Institute of Research and Development, Duy Tan University, Da Nang 550000, Vietnam
[b] Faculty of Electrical – Electronic Engineering, Duy Tan University, Da Nang 550000, Vietnam
[c] Young Researchers and Elite Club, Yasooj Branch, Islamic Azad University, Yasooj, Iran
[d] Department of Mechanical Engineering, Shahid Chamran University of Ahvaz, Ahvaz, Iran
[e] ECAM Lyon, LabECAM, Université de Lyon, Lyon, France
[f] School of Mechanical and Mechatronic Engineering, Faculty of Engineering and Information Technology, University of Technology Sydney, Ultimo, NSW 2007, Australia
[g] Department of Mechanical Engineering, College of Engineering at Wadi Addwaser, Prince Sattam Bin Abdulaziz University, Saudi Arabia
[h] Department of Mechanical Engineering, Faculty of Engineering, University of Khartoum, Sudan
[i] Deptartment of Mathematics, College of Science, King Khalid University, Abha 62529, Saudi Arabia
[j] Department of Mathematics, Faculty of Science, South Valley University, Qena 83523, Egypt

ARTICLE INFO

Article history:
Received 7 September 2020
Received in revised form 19 March 2021
Accepted 8 April 2021
Available online 28 April 2021

Keywords:
Nano-Encapsulated Phase Change Material (NEPCM)
Thermal energy storage
Suspension
Natural convection heat transfer

ABSTRACT

The energy storage capability of a suspension of Nano-Encapsulated Phase Change Material (NEPCM) nanoparticles was addressed in an enclosure during the charging and discharging process. The nanoparticles contain a Phase Change Material (PCM) core, which are capable to absorb a notable quantity of thermal energy on melting. There is a heat pipe in the cavity at the bottom corner, which is enhanced by a layer of metallic matrix. The natural convection flow occurs due to a temperature gradient during the charging or discharging process. The particles of NEPCM move with the natural convection flow and contribute to heat transfer & storage of thermal energy. The regulating equations for the heat transfer & flow of the NEPCM suspension were established & converted in the non-dimensional type. The finite element method (FEM) was utilized in resolving the equations. The results show that there was a rise in the rate of heat transfer & storage of total energy with a rise in nanoparticles volume fraction. The decrease of the Stefan number from 0.2 to 0.6 increases the total stored energy by 25%. The fusion temperature is another important parameter in which its behavior depends on the charging or discharging process.

1. Introduction

The increasing need for the primary power for urbanization and industrialization reached the peak in the previous century, and the recent projection predicts about 40% rise within 2040 [1]. On the contrary, the contribution of the primary energy from fossil fuels is expected to be reduced from 80% to 73% in 2040 [2]. The waste energy in different engineering applications (such as gasoline vehicles 75–82% [3], Lithium-ion battery 10–20% [4], combustion engine 50–90% [5]) are significant as they are not 100% efficient. The growing environmental hazards of overuse of fossil fuels, low availability of natural energy sources, and waste of thermal energy from various engineering systems inspire the scientific community to find out a better thermal management system.

Studies over the past few decades have employed different techniques to minimize thermal energy loss and improved the overall thermal storage system. Various studies have employed sensible heat-storing [6,7] and latent heat-storing [8] systems for the storage of thermal energy. Still, a low volume, high heat storage density, and the ability to stock the heat energy of the fusion at a nearly steady or persistent temperature case similar to the transformation of the phase of the PCM's make latent heat storage technique more efficient for the energy storage system. PCM as heat storage material was first used in the 1940's due to the higher storage capacity of the material [9]. However, one of the PCM's characteristics of low thermal conductivity restricts the thermal operation capacity enhancement for most engineering applications. Studies over the past few decades introduced finned surface

* Corresponding author at: Duy Tan University, Da Nang 550000, Vietnam.
E-mail address: mehdighalambaz@duytan.edu.vn (M. Ghalambaz).

https://doi.org/10.1016/j.apt.2021.04.008

[10,11], bubble agitation [12], and metal foams [5,13,14] to enhance the PCM's thermal performance. Amongst all the heat enhancement techniques, encapsulation becomes the most appropriate method as it improves the higher heat transfer efficiency while it prevents any reaction between the phases. It is evident that leakage could happen at the time of the PCM's phase transformation, which affects the system's overall thermal performance [15].

The encapsulation method potentially solved this problem by wrapping the PCM materials in a capsule core and improved the stability of the thermal system. The stability of the thermal system and the rate of heat transfer varies with the particle size. A study on micro-encapsulated PCM of a pump reports that thermal stability and performance of a system enhanced with a decrease in the micro-particle diameter [16]. The available literature on micro-encapsulation [17,18] reports higher thermal performance for different engineering applications than the other enhancement methods. However, NEPCM is proved as a better method due to its smaller dimension, suspension stability, and larger superficial area for heat transfer.

The unique thermal properties of NEPCM encourage the researchers to perform a variety of numerical [19] and molecular dynamics [20] studies to improve the thermal operation capacity of various engineering structures.

All of the literature studies analyzed the heat transfer by natural convection, & the NEPCM suspension improved overall thermal performance. In recent years, NEPCM's are employed in various heat enhancement techniques. An interfacial polymerization technique used NEPCM for the thermal energy storage of a system [21]. The study concludes that NEPCM is stable with the melting and crystallization enthalpy. An exploratory analysis investigated that thermal performance of a paraffin NEPCM of a pulsating heat pipe and reported lower thermal resistance for the pipe [22].

The thermal ability of a PCMs depends on the proper melting and solidification of the materials. The low conductivity of the organic PCMs influences the overall thermal performance during the discharging and charging process. Some studies [23,24] have investigated the discharging and charging process of the heat storage system. The experimental study used PCM for the fabricated thermal storage system and characterize the thermo-physical properties of the charging and discharging method. A 2-D multiphase model studied the dynamic performance of the storage system of the packed bed type which used encapsulated PCM [25]. An analysis employed macro encapsulated PCM and reported a higher charging and discharging rate of the smaller capsule than the large capsule.

Considering the heat transfer of NEPCM suspensions into a permeable matrix, Ghalambaz et al. [26] examined the natural convection behavior of NEPCMs made of nonadecane core and polyurethane shell. The nanoparticles were suspended in the water, and the permeable medium consisted of the glass balls. These authors employed a lamped model for simulation of the phase change of nanoparticles and investigated the transfer of heat at steady-state convection. The outcomes revealed that dispersing a nanoparticle in water could improve a heat transfer by 13%, and increasing the nanoparticles latent heat might further improve the transfer of heat. Following [26], Ghalambaz et al. [27] explored the heat transfer by steady-state natural convection of NEPCM-water suspensions inside an annulus of the porous eccentric horizontal cylinder. The results of this investigation showed that for the maximum rate of heat transfer there is an optimum fusion temperature which is about a mean temperature of cold & hot walls of an enclosure. The steady-state heat transfer at local thermal non-equilibrium of NEPCM suspensions in the cavity has also been examined recently by Ghalambaz et al. [28]. They reported that NEPCM particles existence could improve the rate of heat transfer by 47%. Additionally, a presence of NEPCMs in a porous medium with poor thermal conductivity was more beneficial compared to high thermal conductive porous materials.

Mehryan et al. [29] researched the impact of utilizing a layer of porous medium & NEPCM-suspension on the steady-state transfer of heat enhancement in an enclosed space. They discovered that a porous layer could effectively contribute to the heat transfer and thermal behavior of NEPCM-suspension. They also reported a scale for the NEPCM particle's optimum fusion temperature. The incidence of the volume fraction of 5% of nanoparticles could improve an overall heat transfer by about 29%.

Most of the literature works have considered the NEPCM-suspensions in the steady-state conditions and investigated the heat transfer in enclosures. The literature evaluation reveals that using the NEPCM-suspensions might improve the heat transfer by the convective way. Though, the thermal energy storage of NEPCM-suspensions during the charging/discharging process is another critical aspect of this suspension. The thermal energy storage of NEPCM-suspensions, which is an unsteady process, has been extensively overlooked in the literature. The current research intends to focus on the thermal charging/discharging nature of NEPCM-suspensions in the enclosure for the first time.

2. Problem physics

Fig. 1 (a), (b), and (c) elaborate the problem physics under investigation along with the boundary conditions. As illustrated in Fig. 1 (a), four chambers surrounding an active tube are full of a suspension, including water and particles of the NEPCM. The nano-additives core material is nonadecane & its shell material is polyurethane (PU). Two different states can be imaged for the studied chamber, as shown in Fig. 1 (b) & (c). In Fig. 1 (b), the temperature of the active wall is greater than compared of the suspension. Thus, a core of nano-additives undergoes melting, and the heat charge state occurs. On the contrary, when the active wall is cold, the cores are solidified, and they release thermal energy. As Fig. 1 (a) illustrates, a porous layer, made of aluminum, has surrounded the active tube. There is no thermal slip between a solid pattern & a suspension of the medium. The properties of components making the suspension are listed in Table 1.

2.1. The formulation

The equations of the continuity, momentum, & energy for the laminar & Newtonian fluid, wherein a density is constant and only varies linearly with the temperature in buoyancy force, are:

$$\frac{\partial u^*}{\partial x^*}+\frac{\partial v^*}{\partial y^*}=0 \tag{1}$$

$$\frac{\rho_b^*}{\varepsilon_i}\frac{\partial u^*}{\partial t^*}+\frac{\rho_b^*}{\varepsilon_i^2}\left(u^*\frac{\partial u^*}{\partial x^*}+v^*\frac{\partial u^*}{\partial y^*}\right)=-\frac{\partial p^*}{\partial x^*}+\frac{\mu_b^*}{\varepsilon_i}\left(\frac{\partial^2 u^*}{\partial x^{*2}}+\frac{\partial^2 u^*}{\partial y^{*2}}\right)-\frac{\mu_b^*}{K_i^*}u^* \tag{2a}$$

$$\frac{\rho_b^*}{\varepsilon_i}\frac{\partial v^*}{\partial t^*}+\frac{\rho_b^*}{\varepsilon_i^2}\left(u^*\frac{\partial v^*}{\partial x^*}+v^*\frac{\partial v^*}{\partial y^*}\right)=-\frac{\partial p^*}{\partial y^*}+\frac{\mu_b^*}{\varepsilon_i}\left(\frac{\partial^2 v^*}{\partial x^{*2}}+\frac{\partial^2 v^*}{\partial y^{*2}}\right)+g^*\rho_b^*\beta_b^*(T^*-T_c^*)-\frac{\mu_b^*}{K_i^*}v^* \tag{2b}$$

$$\left((1-\varepsilon_i)\left(\rho^* C_p^*\right)_s+\varepsilon_i\left(\rho^* C_p^*\right)_b\right)\frac{\partial T^*}{\partial t^*}+\left(\rho^* C_p^*\right)_b\left(u^*\frac{\partial T^*}{\partial x^*}+v^*\frac{\partial T^*}{\partial y^*}\right)=((1-\varepsilon_i)k_s^*+\varepsilon_i k_b^*)\left(\frac{\partial^2 T^*}{\partial x^{*2}}+\frac{\partial^2 T^*}{\partial y^{*2}}\right) \tag{3}$$

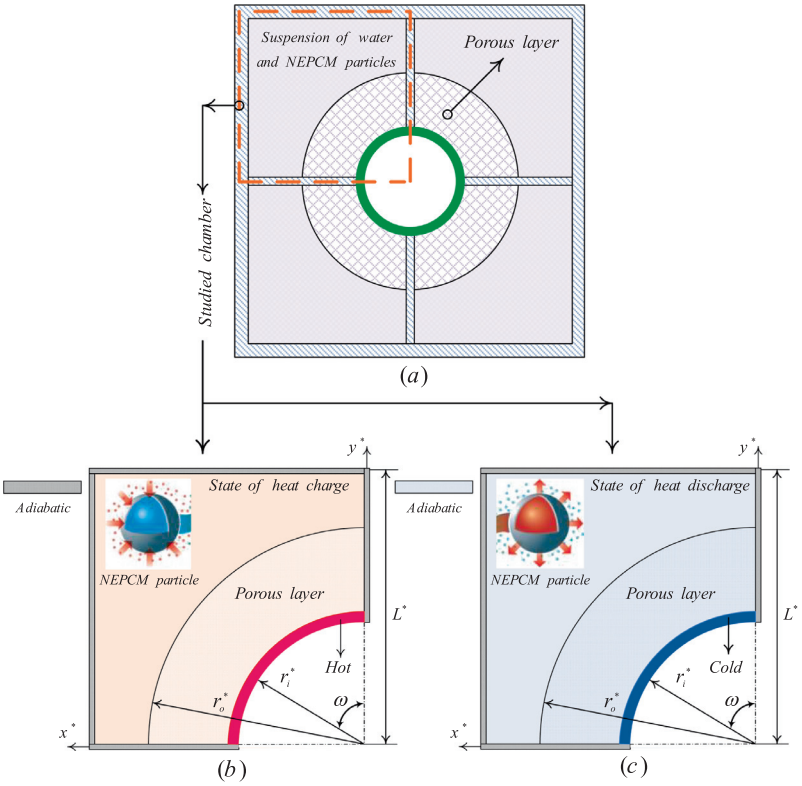

Fig. 1. (a) Graphic design of the problem physics, in which four chambers surround an active tube. The chambers are full of a suspension, including water and particles of the NEPCM. A porous layer, made of aluminum, covered the active tube. Two different states can be imaged for the studied chamber, as shown in Figs. (b) and (c). Fig. (b): Heat charge state; the active wall temperature is greater than that of the suspension. Thus, the core of nano-additives undergoes melting; Fig. (c): Heat discharge state; the active wall temperature is lower than that of the suspension. Thus, the core of nano-additives undergoes solidification.

Table 1
Thermophysical features of the substances [31].

	k (W/m.K)	ρ (Kg/m^3)	C_p (KJ/Kg.K)	β (K^{-1})	μ (kg/m. s)
Host fluid	0.613	997.1	4179	21×10^{-5}	8.9×10^{-4}
PU	–	786	1317.7	17.28×10^{-5}	–
Nonadecane	–	721	2037	–	–
Aluminum	205	2700	897	–	–

where

$$\varepsilon_i = \begin{cases} 1 \ clear\ region \\ \varepsilon \ porouslayer \end{cases} \tag{4a}$$

$$K_i^* = \begin{cases} \infty \ clear\ region \\ K^* \ porouslayer \end{cases} \tag{4b}$$

The corresponding boundary conditions are:

$$\forall\, x^*,\ y^*,\ t^* \ \left| y^{*^2}, x^{*^2} = r_i^{*^2},\ y^* \geqslant 0,\ x^* \geqslant 0,\ t^* \geqslant 0 \right. \Rightarrow u^* = v^* = 0,\ T_i^* = \begin{cases} T_h^* \text{ heat charge state} \\ T_c^* \text{ heat discharge state} \end{cases} \tag{5a}$$

$$\forall\, x^*,\ y^*,\ t^* \ \left| r_i^* \leqslant x^* \leqslant L^*,\ y^* = 0,\ t^* \geqslant 0 \right. \Rightarrow u^* = v^* = 0,\ \frac{\partial T^*}{\partial y^*} = 0 \tag{5b}$$

$$\forall\, x^*,\ y^*,\ t^* \ \left| r_i^* \leqslant y^* \leqslant L^*,\ x^* = 0,\ t^* \geqslant 0 \right. \Rightarrow u^* = v^* = 0,\ \frac{\partial T^*}{\partial x^*} = 0 \tag{5c}$$

$$\forall\, x^*,\ y^*,\ t^* \ \left| 0 \leqslant x^* \leqslant L^*,\ y^* = L^*,\ t^* \geqslant 0 \right. \Rightarrow u^* = v^* = 0,\ \frac{\partial T^*}{\partial y^*} = 0 \tag{5d}$$

$$\forall\, x^*,\ y^*,\ t^* \ \left| x^{*^2} + y^{*^2} = r_o^{*^2},\ x^* \geqslant 0,\ y^* \geqslant 0,\ t^* \geqslant 0 \right. \Rightarrow u_{CR}^* = u_{PL}^*,\ v_{CR}^* = v_{PL}^*,\ \frac{\mu_b^*}{\varepsilon_i}\frac{\partial u^*}{\partial n^*}\Big|_{CR} = \frac{\mu_b^*}{\varepsilon_i}\frac{\partial u^*}{\partial n^*}\Big|_{PL},\ \frac{\mu_b^*}{\varepsilon_i}\frac{\partial v^*}{\partial n^*}\Big|_{CR} = \frac{\mu_b^*}{\varepsilon_i}\frac{\partial v^*}{\partial n^*}\Big|_{PL},\ k_b^*\frac{\partial T^*}{\partial n^*}\Big|_{CR} = \left((1-\varepsilon)k_s^* + \varepsilon k_b^*\right)\frac{\partial T^*}{\partial n^*}\Big|_{PL},\ T^*|_{CR} = T^*|_{PL} \tag{5e}$$

Also, the initial condition is as follows:

$$\forall\, x^*,\ y^*,\ t^* \mid 0 < x^* < L^*,\ 0 < y^* < L^*,\ t^* = 0 \Rightarrow u^* = v^* = 0,\ T^* = \begin{cases} T_c^* \ heat\ charge\ state \\ T_h^* \ heat\ discharge\ state \end{cases} \tag{5f}$$

2.2. Effective characteristics of the suspension

The density of the mixture, as a function of the densities of the nano-additives and the base fluid, is [30]:

$$\rho_b^* = (1-\phi)\rho_f^* + \phi\rho_p^* \tag{6}$$

The density of nano-additives is as follow:

$$\rho_p^* = \left(\rho_{sh}^* + \imath\rho_{co}^*\right)^{-1}(1+\imath)\rho_{co}^*\rho_{sh}^* \tag{7}$$

in which, $\imath$ is about 0.447 [31]. The mixtures total heat capacity, which includes sensible heat capacities of a host fluid & nano-additives & a latent heat of nano-additives is [32,33]:

Table 2
The comparison among the mean Nusselt number of different grid cases.

Cases	Number of elements	Nu_a	Δ_i (%)	Time to run
Case I	7516	46.491		2min 19s
Case II	18070	46.506	0.032264	5min 21s
Case III	30122	46.576	0.150518	31min 10s
Case IV	**48420**	**46.621**	**0.096616**	**38min 46s**
Case V	62416	46.632	0.023595	52min 41s

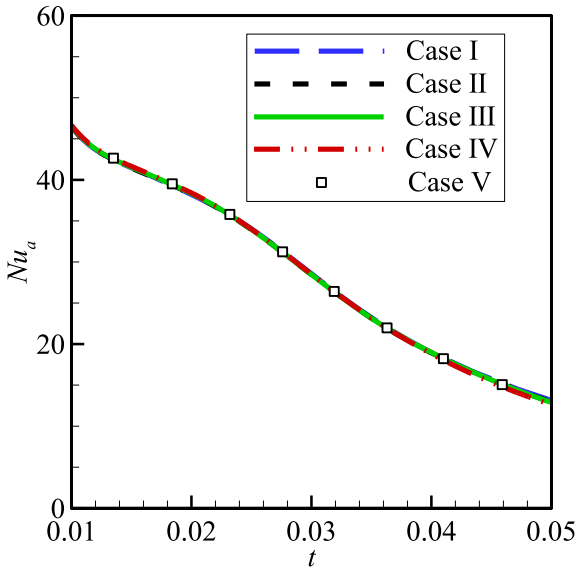

Fig. 2. The reliance of the Nu_a to the grid of the different sizes; Case I (7516 elements), Case II (18070 elements), Case III (30122 elements), Case IV (48420 elements), Case V (62416 elements). As clearly shown, Nu_a is not substantially influenced by the grid size. As seen, the results change minimally (≈ 0.1%) for the cases IV and V.

$$C^*_{p,b} = \rho^{*-1}_b \phi\left(\rho^*_p C^*_{p,p,eff} - \rho^*_f C^*_{p,f}\right) + \rho^*_f C^*_{p,f} \tag{8a}$$

The effective heat capacity of an encapsulated nano-additives without the phase change of a core is equal to a sensible heat capacity of nano-additives [33]:

$$C^*_{p,p} = (1+\imath)^{-1}\left(C^*_{p,co} + \imath C^*_{p,sh}\right) \tag{8b}$$

The effective heat capacity of nano-additives with a phase change of a core is defined as the following [30,34]:

$$C^*_{p,p,eff} = C^*_{p,p} + \left\{\frac{\pi}{2}\cdot\left(\frac{h^*_{sf}}{T^*_{Mr}} - C^*_{p,p}\right)\cdot\sin\left(\pi\frac{T^* - T^*_{fu} + T^*_{Mr}/2}{T^*_{Mr}}\right)\right\}\gamma$$
$$\gamma = \begin{cases} 0 & T^* < T^*_{fu} - T_{Mr}/2 \\ 1 & T_{fu} - T^*_{Mr}/2 < T^* < T^*_{fu} + T^*_{Mr}/2 \\ 0 & T^* > T^*_{fu} + T^*_{Mr}/2 \end{cases} \tag{9}$$

The coefficient of thermal volume expansion of a mixture is [33]:

$$\beta^*_b = (1-\phi)\beta^*_f + \phi\beta^*_p \tag{10}$$

The following relations can be utilized to obtain a thermal conductivity and dynamic viscosity of a mixture:

$$k^*_b = k^*_f(1 + Nc\phi) \tag{11a}$$

$$\mu^*_b = \mu^*_f(1 + N\nu\phi) \tag{11b}$$

Nc & *Nv*, respectively, are the number of thermal conductivity & dynamic viscosity.

2.3. Normalized form of the equations

A non-dimensional format of governing equations and the associated boundary conditions can be obtained by using the following non-dimensional parameters:

$$x = \frac{x^*}{L^*},\ y = \frac{y^*}{L^*},\ r_i = \frac{r^*_i}{L^*},\ r_o = \frac{r^*_o}{L^*},\ u = \frac{u^*L^*}{\alpha^*_f}$$
$$v = \frac{v^*L^*}{\alpha^*_f},\ p = \frac{p^*L^{*2}}{\rho^*_f\alpha^{*2}_f},\ T = \frac{T^* - T^*_c}{T^*_h - T^*_c},\ t = \frac{\alpha^*_f t^*}{L^2} \tag{12}$$

where the ultimate non-dimensional shape of equations is:

$$\frac{\partial u}{\partial x} + \frac{\partial v}{\partial y} = 0 \tag{13}$$

$$\frac{\rho_r}{\varepsilon_i}\frac{\partial u}{\partial t} + \frac{\rho_r}{\varepsilon_i^2}\left(u\frac{\partial u}{\partial x} + v\frac{\partial u}{\partial y}\right) = -\frac{\partial p}{\partial x} + Pr\frac{\mu_r}{\varepsilon_i}\left(\frac{\partial^2 u}{\partial x^2} + \frac{\partial^2 u}{\partial y^2}\right) - Pr\frac{\mu_r}{Da_i}u \tag{14}$$

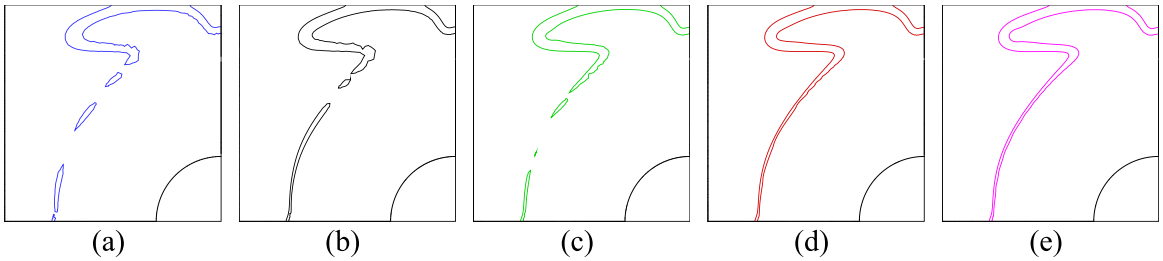

Fig. 3. Dependency of Cr_b to the grid size (a) Case I (7516 elements), (b) Case II (18070 elements), (c) Case III (30122 elements), (d) Case IV (48420 elements) and (e) Case V (62416 elements) when t = 0.01, λ = 0.3225, Ste = 0.2, θ_f = 0.1, ϕ = 0.05, Da = 3.41 × 10^{-4} and Ra = 10^6. As seen, the figures of case IV and case V show similar results. In addition, the phase change zone is fully continuous for the grid of Case IV. Therefore, according to Fig. 3 and Table 2, case IV was considered for numerical studies to save time and computational cost.

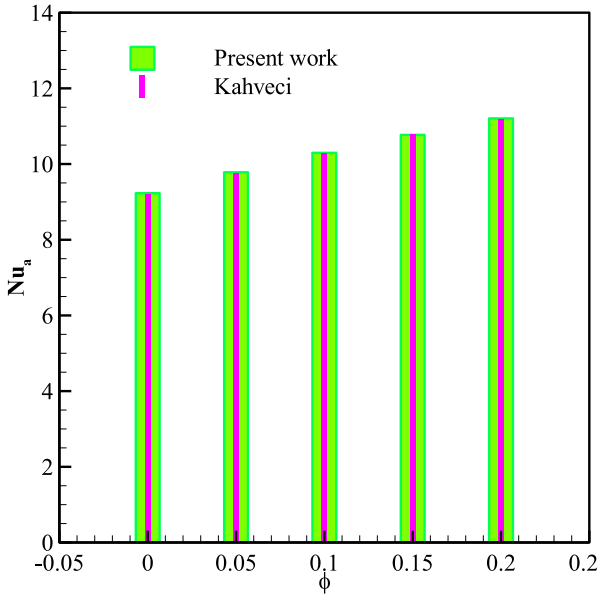

Fig. 4. To verify the natural convection of nanofluid of this research, the comparison of the results of the average Nusselt number of present work with green color and Kahveci [36] with violet color is made. Kahveci [36] investigated the natural convection of nanofluid within a square enclosure for the various volume fraction of nanoparticles. Two walls of the cavity were adiabatic, and two of them were isothermal at temperatures of T_h and T_c. Five types of nanoparticles in a range of 0–20% were examined in his investigations that TiO_2 was chosen as the validation case. The results are reported at $Ra = 10^6$ and $Pr = 0.6$ for different volume fractions, which show a good agreement. (For interpretation of the references to color in this figure legend, the reader is referred to the web version of this article.)

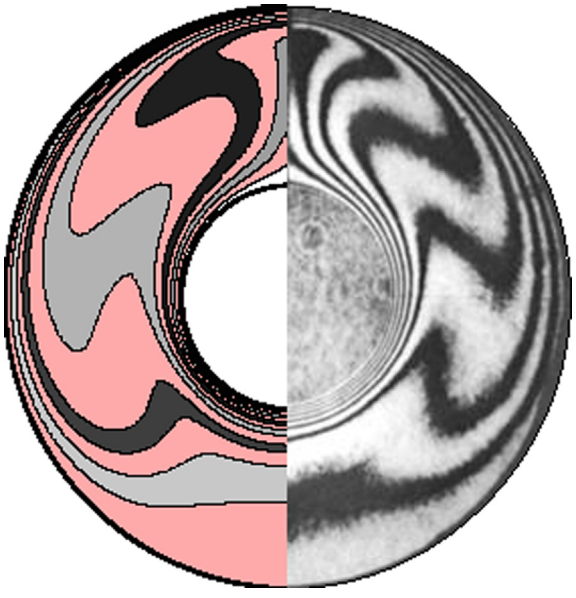

Fig. 5. To validate the natural convection mechanism of this study, the results of this study (left) were evaluated with the experimental research of Goldstein & Kuehn [37] (right). They did experimental and analytical investigations to examine the natural convection inside a horizontal annulus. The working fluid of their study was air. According to the figure, which demonstrates the isotherms of this study (left) and those of Kuehn and Goldstein [37] (right) at $Pr = 0.706$ and $Ra = 4.7 \times 10^4$, a good agreement was achieved.

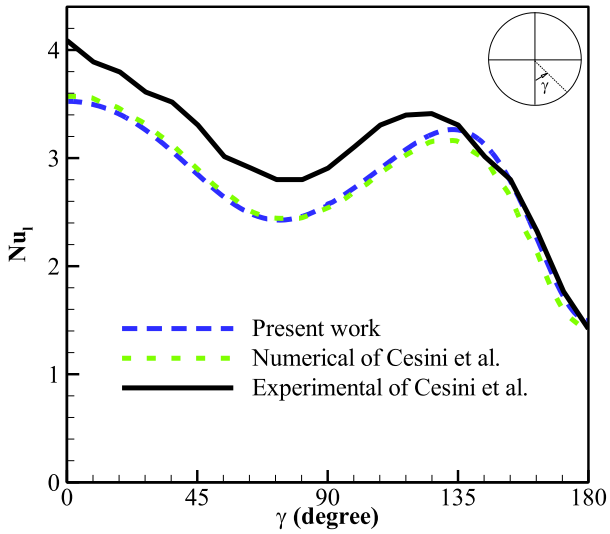

Fig. 6. The comparison between the local Nusselt number at different positions around the cylinder in the present work that show with dashed blue color and the research of Cesini et al. [38] that they experimentally show with solid black color and numerically with green color, studied the natural convection heat transfer of a horizontal cylinder trapped in a rectangular cavity. The results are reported at $Ra = 2.4 \times 10^3$. (For interpretation of the references to color in this figure legend, the reader is referred to the web version of this article.)

Table 3
The comparison among the outcomes of present work & Ref. [55] for the mean Nusselt number of a porous medium inside a rectangular cavity when $Pr = 1$.

Da	Ra	ε	Nu_a (present work)	Nu_a (Ref. [39])	Error%
10^{-6}	10^7	0.4	1.078	1.078	0
10^{-4}	10^7	0.9	9.322	9.202	1.3
10^{-2}	10^4	0.4	1.360	1.408	3.4
10^{-2}	10^5	0.9	3.92	3.91	0.2

$$\frac{\rho_r}{\varepsilon_i}\frac{\partial v}{\partial t}+\frac{\rho_r}{\varepsilon_i^2}\left(u\frac{\partial v}{\partial x}+v\frac{\partial v}{\partial y}\right)=-\frac{\partial p}{\partial y}+Pr\frac{\mu_r}{\varepsilon_i}\left(\frac{\partial^2 v}{\partial x^2}+\frac{\partial^2 v}{\partial y^2}\right)-Pr\times\frac{\mu_r}{Da_i}v+Ra\cdot Pr\beta_r\rho_r T \tag{15}$$

where

$$Ra=\frac{g^*\rho_f^*\beta_f^*(T_h^*-T_c^*)L^{*3}}{\alpha_f^*\mu_f^*},\quad Pr=\frac{\mu_f^*}{\rho_f^*\alpha_f^*},\quad Da_i=\frac{K_i^*}{L^{*2}}=\begin{cases}\infty\ Clear\ region\\ Da\ Porous\ layer\end{cases} \tag{16a}$$

$$\rho_r=\left(\frac{\rho_b^*}{\rho_f^*}\right)=(1-\phi)+\phi\left(\frac{\rho_p^*}{\rho_f^*}\right),\quad \beta_r=\left(\frac{\beta_b^*}{\beta_f^*}\right)=(1-\phi)+\phi\left(\frac{\beta_p^*}{\beta_f^*}\right),\quad \mu_r=\left(\frac{\mu_b^*}{\mu_f^*}\right)=1+N\nu\phi \tag{16b}$$

Finally, the thermal expansions of the NEPCM particles and host fluid (water) are assumed to be the same, therefore, $\beta_r = 1$.

$$((1-\varepsilon_i)Cr_s+\varepsilon_i Cr_b)\frac{\partial T}{\partial t}+Cr_b\left(u\frac{\partial T}{\partial x}+v\frac{\partial T}{\partial y}\right)=((1-\varepsilon_i)k_{rs}+\varepsilon_i k_{rb})\left(\frac{\partial^2 T}{\partial x^2}+\frac{\partial^2 T}{\partial y^2}\right) \tag{17}$$

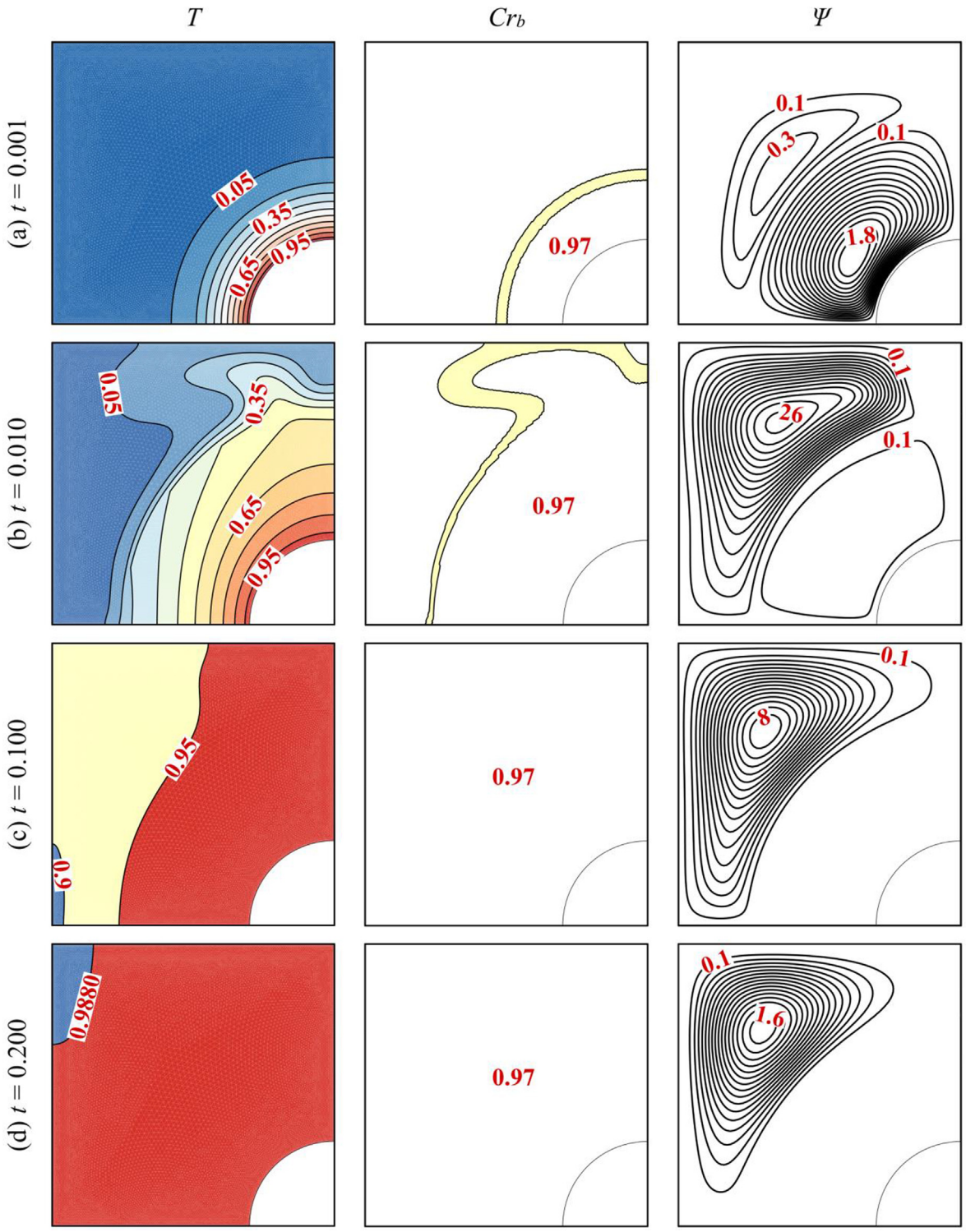

Fig. 7. The Isotherm, Heat capacity ratio and streamlines during times from $t = 0.001$ to $t = 0.2$ when $\lambda = 0.3225$, $Ste = 0.2$, $T_{fu} = 0.1$, $\phi = 0.05$, $Da = 3.41 \times 10^{-4}$ and $Ra = 10^6$. At $t = 0.2$. It is clear that the phase change zone follows the development of the isothermal contours and coincides with the isotherm corresponding to the fusion temperature. As the temperature of the fluid increases in the cavity, the phase change zone shifts away from the inner heater before finally disappearing when all the fluid in the cavity has reached the maximum temperature, and the totality of the NEPCM cores have melted.

where

$$Cr_b = \frac{\left(\rho^* C_p^*\right)_b}{\left(\rho^* C_p^*\right)_f} = (1-\phi) + \phi\lambda + \frac{\phi}{\delta\, Ste} f,$$
$$Cr_s = \frac{\left(\rho^* C_p^*\right)_s}{\left(\rho^* C_p^*\right)_f}, \quad k_{rb} = \frac{k_b^*}{k_f^*} = 1 + Nc\phi, \; k_{rs} = \frac{k_s^*}{k_f^*} \tag{18}$$

In the above equations, Ste, λ, and T_{Mr} are as the following:

$$Ste = \frac{\left(\rho^* C_p^*\right)_f (T_h^* - T_c^*)\left(\rho_{sh}^* + \imath\rho_{co}^*\right)}{h_{sf}^* \rho_{co}^* \rho_{sh}^*},$$
$$\lambda = \frac{\left(C_{p,co}^* + \imath C_{p,sh}^*\right)\rho_{co}^* \rho_{sh}^*}{\left(\rho^* C_p^*\right)_f \left(\rho_{sh}^* + \imath\rho_{co}^*\right)}, \; T_{Mr} = \frac{T_{Mr}^*}{(T_h^* - T_c^*)} \tag{19}$$

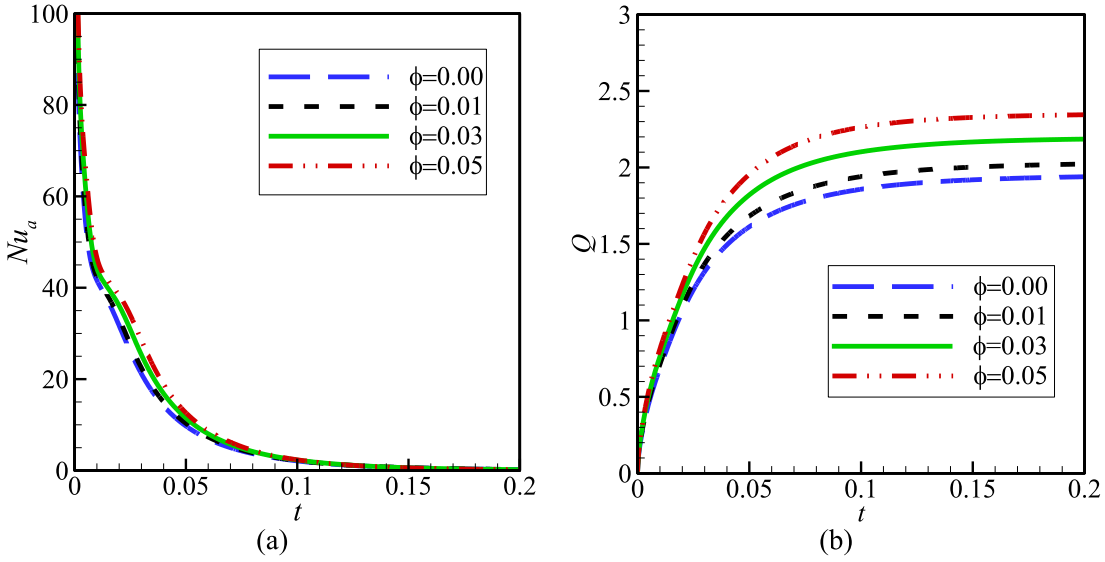

Fig. 8. The impact of different concentrations of the NEPCM particles on (a) Nusselt number (Nu_a) (b) Q during non-dimensional time when λ = 0.3225, Ste = 0.2, T_{fu} = 0.1, $Da = 3.41 \times 10^{-4}$ and $Ra = 10^6$. Utilizing a greater concentration of the NEPCM particles means that more particles are undergoing phase change and increases the contribution of the NEPCM to the total heat transfer occurring in the cavity and consequently raises the values of Nu_a and Q.

which Ste is Stefan number, λ is a ratio of sensible heat capacity, & T_{Mr} is an interval of normalized melting. Also, f is:

$$f = \frac{\pi}{2}\sin\left(\frac{\pi}{T_{Mr}}(T - T_{fu} + T_{Mr}/2)\right)\sigma,$$
$$\sigma = \begin{cases} 0 & T < T_{fu} - T_{Mr}/2 \\ 1 & T_{fu} - T_{Mr}/2 < T < T_{fu} + T_{Mr}/2 \\ 0 & T > T_{fu} + T_{Mr}/2 \end{cases} \quad (20)$$

which f is the normalized fusion function. T_{fu} of Eq. (20) is the normalized fusion temperature:

$$T_{fu} = \frac{T^*_{fu} - T^*_c}{T^*_h - T^*_c} \quad (21)$$

The normalized format of the boundary and initial conditions are as the following:

$$\forall\ x,\ y,\ t\ |x^2 + y^2 = r_i^2,\ x \geqslant 0,\ y \geqslant 0,\ t \geqslant 0 \ \Rightarrow u = v = 0,\ T_i = \begin{cases} 1 \text{ heat charge state} \\ 0 \text{ heat discharge state} \end{cases} \quad (22a)$$

$$\forall\ x,\ y,\ t\ |r_i \leqslant x \leqslant 1,\ y = 0,\ t \geqslant 0 \ \Rightarrow u = v = 0,\ \frac{\partial T}{\partial y} = 0,\ \Psi = 0 \quad (22b)$$

$$\forall\ x,\ y,\ t\ |r_i \leqslant y \leqslant 1,\ x = 0,\ t \geqslant 0 \ \Rightarrow u = v = 0,\ \frac{\partial T}{\partial x} = 0,\ \Psi = 0 \quad (22c)$$

$$\forall\ x,\ y,\ t\ |0 \leqslant x \leqslant 1,\ y = L,\ t \geqslant 0 \ \Rightarrow u = v = 0,\ \frac{\partial T}{\partial y} = 0,\ \Psi = 0 \quad (22d)$$

$$\forall\ x,\ y,\ t\ |x^2 + y^2 = r_o^2,\ x \geqslant 0,\ y \geqslant 0,\ t \geqslant 0 \ \Rightarrow u_{CR} = u_{PL}\ ,\ v_{CR} = v_{PL}, \frac{1}{\varepsilon_i}\frac{\partial u}{\partial n}\bigg|_{CR} = \frac{1}{\varepsilon_i}\frac{\partial u}{\partial n}\bigg|_{PL}\ ,\ \frac{1}{\varepsilon_i}\frac{\partial v}{\partial n}\bigg|_{CR} = \frac{1}{\varepsilon_i}\frac{\partial v}{\partial n}\bigg|_{PL},\ T|_{CR} = T|_{PL},\ k_{rb}\frac{\partial T}{\partial n}\bigg|_{CR} = ((1-\varepsilon)k_{rs} + \varepsilon k_{rb})\frac{\partial T}{\partial n}\bigg|_{PL} \quad (22e)$$

$$\forall\ x,\ y,\ t\ \left|\begin{array}{l} 0 < y < 1,\ 0 < x < 1,\ t = 0 \Rightarrow u = v = 0, \\ \begin{cases} T = 0 \text{ if } \forall\ x,\ y\ |x^2 + y^2 = r_i^2 \ \Rightarrow\ T = 1 \\ T = 1 \text{ if } \forall\ x,\ y\ |x^2 + y^2 = r_i^2 \ \Rightarrow T = 0 \end{cases} \end{array}\right. \quad (22f)$$

The energy conservation on an active wall leads to the following:

$$Nu_l = -((1-\varepsilon_i)k_{rs} + \varepsilon_i(1 + Nc\phi))\left(\frac{\partial T}{\partial n}\right)_{x^2+y^2=r_i^2} \quad (23)$$

The integration of the above equations alone with the active wall presents the total heat transfer rate:

$$Nu_a = \frac{2}{\pi}\int_0^{\pi/2} Nu_l d\omega \quad (24)$$

The energy stored/released in the enclosure can be computed by the amount of the transferred energy from the energy source (hot/cold inner wall) as follows:

$$Q = \int_o^{\tau} Nu_a d\tau \quad (25)$$

Streamlines as the path of the suspension in the flow are defined by the use of the following:

$$\frac{\partial^2 \Psi}{\partial x^2} + \frac{\partial^2 \Psi}{\partial y^2} = -\left(\frac{\partial v}{\partial x} - \frac{\partial u}{\partial y}\right) \quad (26)$$

where zero Ψ was applied at the walls.

3. Numerical approach and grid test

3.1. Numerical method

The Galerkin finite element method (FEM) was used to integrate Eqs. (13)-(15) and 26. These equations were written into a weak formulation before utilizing this method. Galerkin finite element method is completely described in [35].

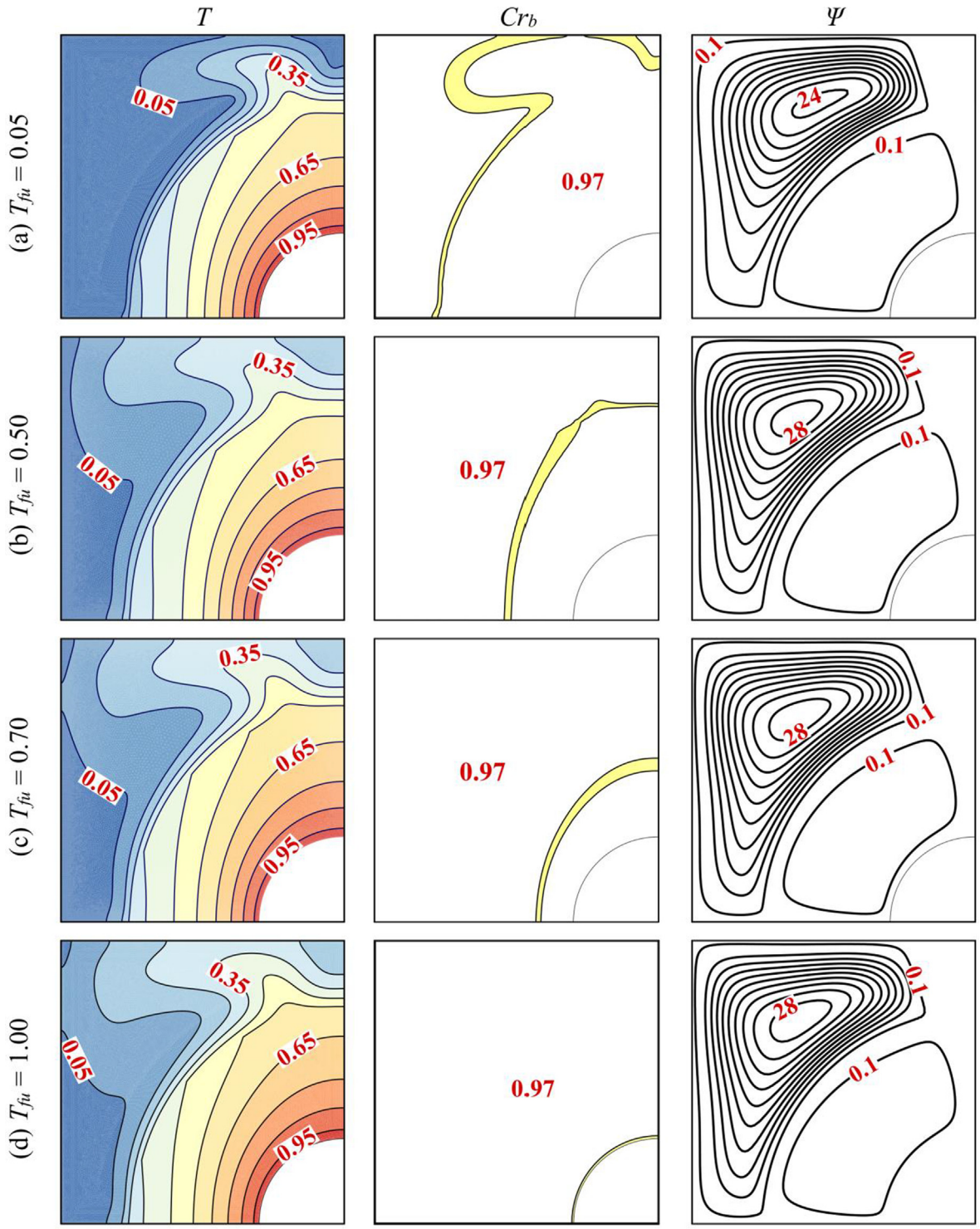

Fig. 9. The isotherm contours, Heat capacity ratio and Streamlines for four non-dimensional fusion temperatures of (a) T_{fu} = 0.05, (b) T_{fu} = 0.50, (c) T_{fu} = 0.70 and (d) T_{fu} = 1.00 in specific time t = 0.01 when λ = 0.3225, ϕ = 0.05, Ste = 0.2, Da = 3.41 × 10^{-4} and Ra = 10^6. Increasing T_{fu} shifts the low-temperature isotherms away from the inner heater and raises the overall temperature of the fluid in the cavity. The contours of show that the zone at which the core of the NEPCM particles undergoes melting varies according to the corresponding isotherm.

3.2. Grid study

The quality grid is a vital part of a numerical investigation to achieve accurate results. So, five different element numbers were provided to examine the grid independence of this study. Table 2 demonstrates a value of mean Nusselt number, i.e., Nu_a at the hot wall for different grid-cases in particular time-step (t = 0.01), when λ = 0.3225, Ste = 0.2, T_{fu} = 0.1, ϕ = 0.05, Da = 3.41 × 10^{-4} and Ra = 10^6. It can be seen that employing a higher number of elements leads to a longer time of simulations. The variation of the results for cases IV and V is negligible (≈ 0.1%). The deviations of mean Nu_a by the time for the various cases are depicted in Fig. 2.

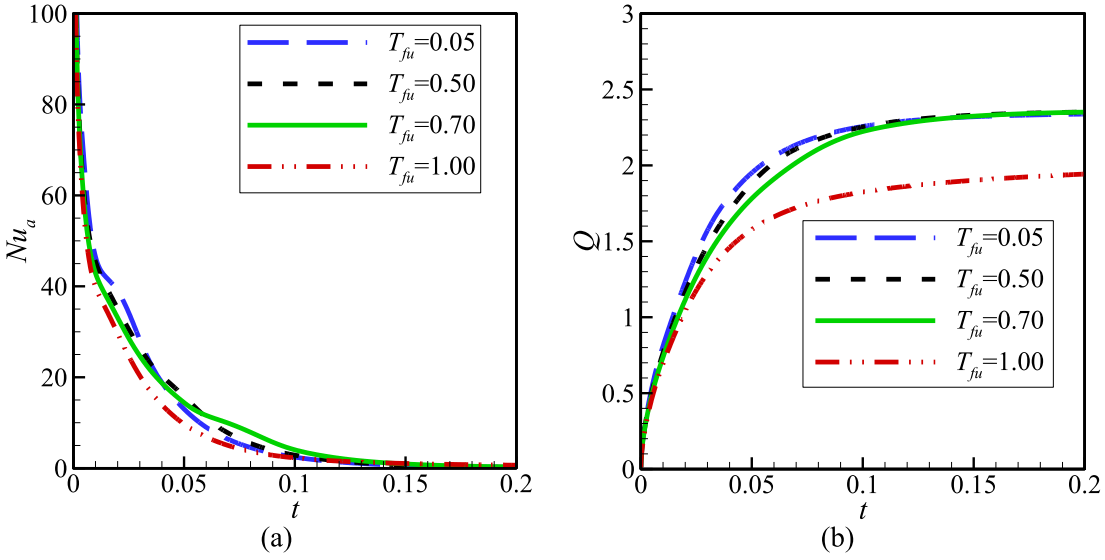

Fig. 10. The effect of different values of non-dimensional fusion temperature on (a) Nusselt number (Nu_a) (b) Q during non-dimensional time when λ = 0.3225, Ste = 0.2, ϕ = 0.05, Da = 3.41 × 10^{-4} and Ra = 10^6. Nu_a illustrates a similar style of deviation for all the values of T_{fu}, while being slightly lower for T_{fu} = 1. The highest value of Nu_a slightly fluctuates between different values of T_{fu}, while Nu_a is always minimum for T_{fu} = 1 compared to the other values. A similar tendency can be seen for Q, which is always a minimum for T_{fu} = 1.

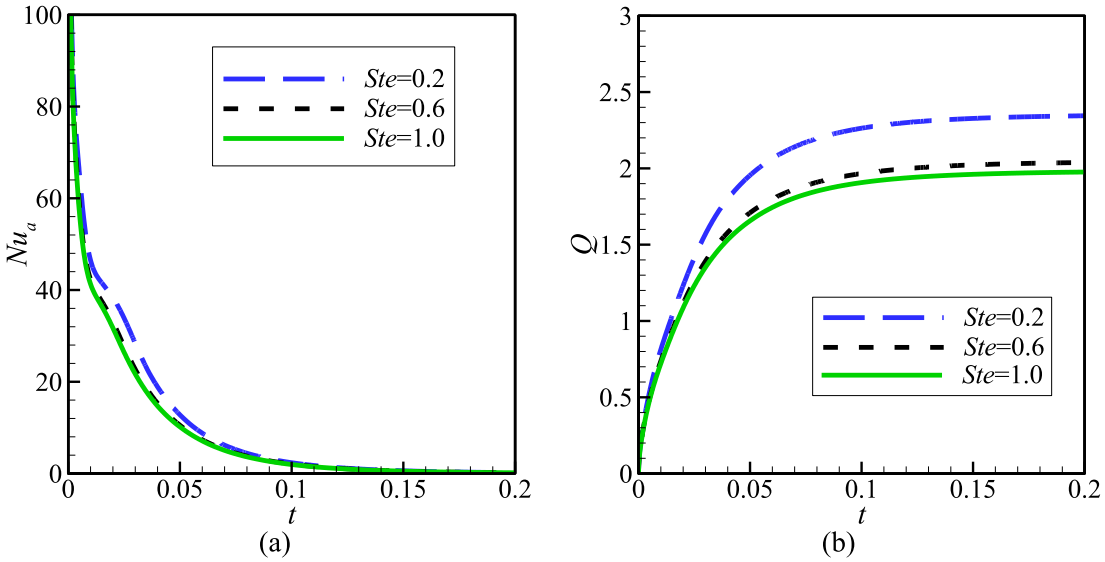

Fig. 11. The impact of different values of Ste number on (a) Nusselt number (Nu_a) (b) Q during non-dimensional time when λ = 0.3225, T_{fu} = 0.1, ϕ = 0.05, Da = 3.41 × 10^{-4} and Ra = 10^6. Since the latent heat of the core of the nano-additives rises when Ste is decreased, and the total heat transfer is enhanced, therefore a reduction of Ste promotes Nu_a and Q.

There is not one considerable dissimilarity among the values of all cases. Furthermore, according to Fig. 3, the heat capacity ratio of all five cases were provided at a specific dimensionless time (t = 0.01), when λ = 0.3225, Ste = 0.2, T_{fu} = 0.1, ϕ = 0.05, Da = 3.41 × 10^{-4} and Ra = 10^6. As seen, the figures of case IV (Fig. 3d) and case V (Fig. 3e) show similar results. Therefore, case IV was considered for numerical studies to save the computational time and costs.

$$\Delta_i = \left|\frac{Nu_{a,i+1} - Nu_{a,i}}{Nu_{a,i}}\right| \times 100 \quad (27)$$

3.3. Comparison with others

To analyze the correctness and precision of an outcome of this study, there must be a resemblance amongst the outcomes of this & other researches. First, the outcomes of the present work were validated by the study of Kahveci [36]. He investigated nanofluids with natural convection within a square enclosure for the nanoparticles of various volume fractions. Two walls of a cavity were adiabatic, & two of them were isothermal at temperatures of T_h and T_c. Five types of nanoparticles in a range of 0–20% were examined in his investigations that TiO_2 was chosen as the validation case. Fig. 4 represents the mean Nu_a of the present work and [36] for different volume fractions, which shows a good agreement.

Second, to verify the natural convection mechanism of this study, the results of this study were equated along with the research of Goldstein & Kuehn [37]. They did experimental and analytical investigations to study the natural convection inside a horizontal annulus. The working fluids of their study were water and air, and the ratio of gap width to inner-cylinder diameter was 0.8. The temperatures of an outer-cylinder & an inner-cylinder walls were T_c & T_h, respectively. According to Fig. 5, which

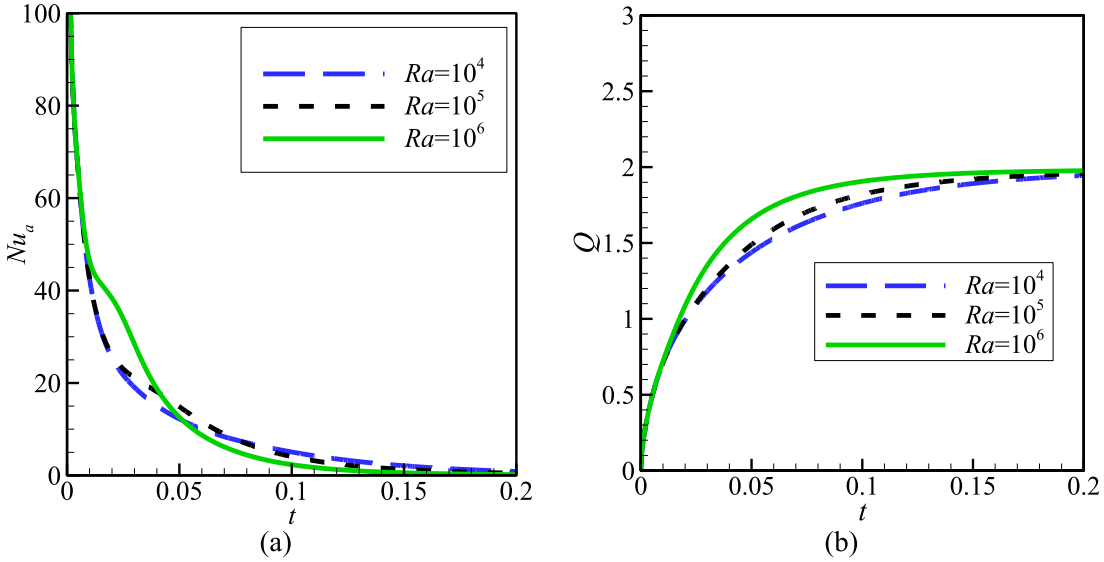

Fig. 12. The impact of different values of *Ra* number on (a) Nusselt number (Nu_a) (b) *Q* through non-dimensional time when λ = 0.3225, *Ste* = 0.2, T_{fu} = 0.1, ϕ = 0.05 and *Da* = 3.41 × 10^{-4}. Raising *Ra* tends to increase Nu_a, and as time passes, the impact of *Ra* becomes less important when the local temperature has reached its maximum. On the other hand, *Q* rises when a greater value of *Ra* is utilized.

demonstrates the isotherms of this study (left) and those of [37] (right), a good agreement was achieved.

Third, the findings of a current research were equated with the work of Cesini et al. [38]. They experimentally and numerically studied the heat transfer by natural convection for the horizontal cylinder trapped inside the rectangular cavity. The air was the heat transfer medium. Two side walls of the enclosure were considered at constant cold temperature (T_c), and the cylinder surface was at a hot isothermal temperature ($T_h > T_c$) while the cavity's lower wall was adiabatic, while the heat flux from a cavity to ambient was taken into account from the upper wall. Fig. 6 indicates a local Nu_a at various positions around the cavity of this study and [38]. The required agreement is seen amongst the findings of the researches.

Finally, a comparison amongst the outcomes of this research & Nithiarasu et al. [39] was provided. They analytically examined the heat transfer by natural convection within the rectangular porous medium. An adiabatic condition was considered for horizontal walls, and isotherm conditions of T_h and T_c were adopted for the vertical walls. Their investigations were done for different *Da*, *Ra,* and ε when Prandtl number is 1. Equating the Nu_a for different values of parameters (Table 3) indicates an excellent agreement among the outcomes of the two types of research.

4. Results and discussion

This section presents the outcomes of modeling the natural convection of a mixture wherein the host fluid is water, and the dispersed particles are nano- additives of the encapsulated PCM in the process of charging and discharging. The core of the nano-encapsulated PCM can experience melting and solidification.

Regarding the study done by Barlak et al. [31] λ = 0.32. Darcy number and porosity are 3.41 × 10^{-4} and 0.95, respectively. Furthermore, *Nc* and *Nv* are considered to be 23.8 and 12.5. The dependency of the temperature field, streamlines, Cr_b field, the rates of heat transfer, & the over-all energy stored to the following parameters are investigated in this work: Rayleigh number ($10^4 \le Ra \le 10^6$), the nano-additives with the volume fraction ($0.0 \le \phi \le 5\%$), Stefan number ($0.2 \le Ste \le 1$), & non-dimensional fusion temperature ($0.05 \le T_{fu} \le 1$).

4.1. Melting result (charging state)

First, the charging state where a temperature of an inner wall is greater compared to a fusion temperature of a core of the nano-additives is considered. In this case, the core of the nano-additives undergoes melting. Fig. 7 depicts the time evolution of the isothermal contours, the heat capacity ratio, i.e., Cr_b, and the streamlines inside the cavity. Initially, the fluid in contact with the active wall starts to heat up, and the temperature in the porous layer surrounding this wall increases and remains higher than the rest of the cavity. The hot fluid moves upwards while the colder one moves down, and convective flow progressively takes place. The streamlines are concentrated near the inner tube, indicating an intense flow in that region. As time passes, the temperature of the fluid in the cavity increases, and convective effects dominate throughout the cavity, motivated by the temperature variance amongst a cold fluid & a hotter one in the vicinity of the inner heater. As the high temperature of the fluid near the inner heater becomes uniform, the convective flow in that region vanishes and becomes primarily intense near the outer walls. Finally, the hot fluid fills most of the cavity, and the natural convection is weakened. As for the Cr_b contours, it should be noted that the thin yellow ribbon in the figure resembles a region where a core of nano-additives goes through the phase transformation. The phase change zone follows the development of the isothermal contours and coincides with the isotherm corresponding to the fusion temperature, i.e., T_{fu}. As the temperature of the fluid rises inside the cavity, the phase change zone shifts away from the inner heater before finally disappearing when all the fluid in the cavity has reached the maximum temperature, and the totality of the NEPCM cores have melted.

Fig. 8 depicts the differences of a mean Nu_a, & total energy transferred from the hot wall, i.e., *Q*, as characteristics of time for various amounts of a volume fraction of the nano-additives, i.e., ϕ. For all the values of ϕ, Nu_a is at its highest at *t* = 0 then decreases with time until reaching zero in the steady part when all the fluid

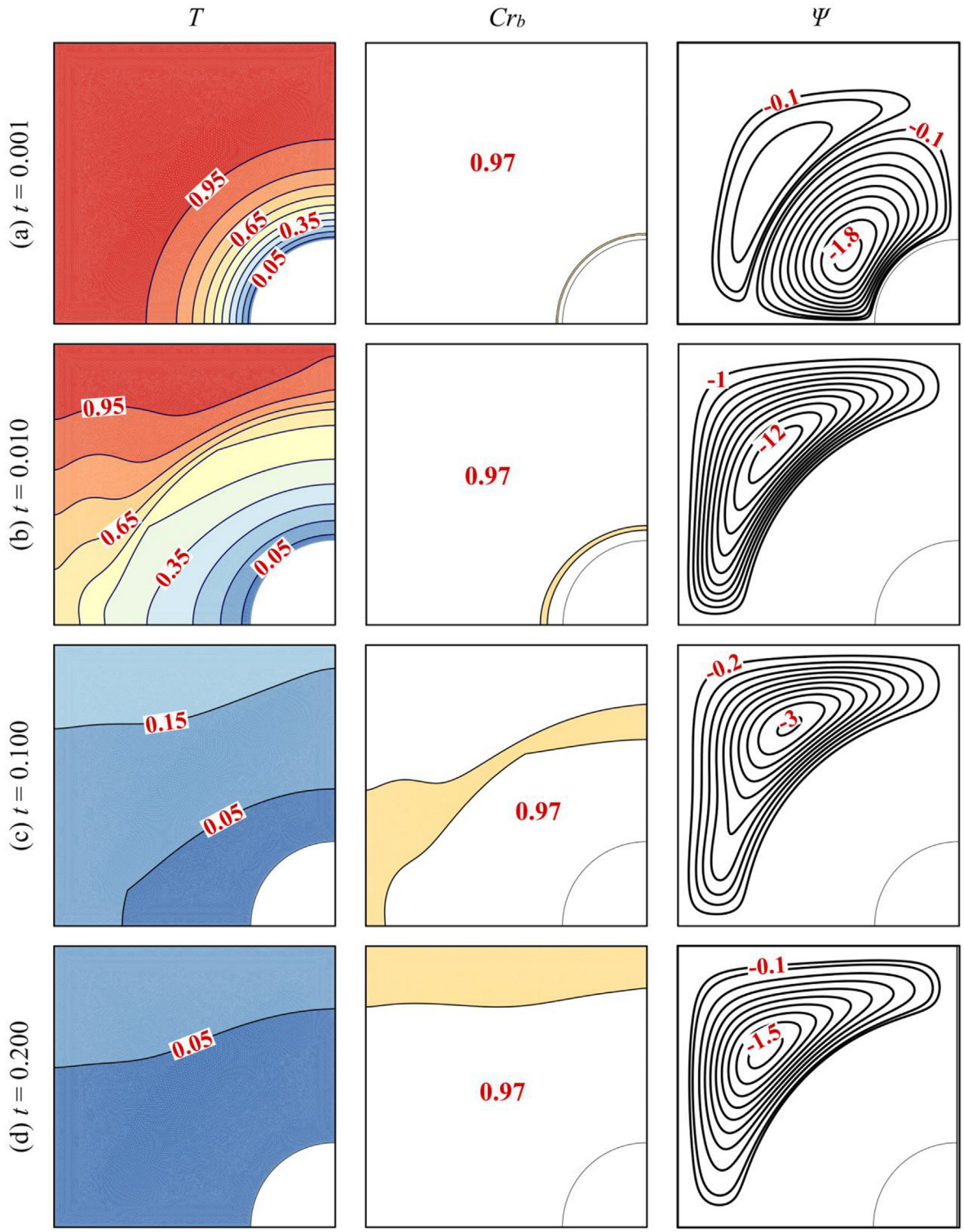

Fig. 13. The Isotherm, heat capacity ratio and Streamlines during times from $t = 0.001$ to $t = 0.2$ when $\lambda = 0.3225$, $Ste = 0.2$, $T_{fu} = 0.1$, $\phi = 0.05$, $Da = 3.41 \times 10^{-4}$ and $Ra = 10^6$. The intensity of the convective flow grows at the beginning near the inner tube, and then, in the upper left part of the cavity, before gradually diminishing when the fluid temperature becomes uniform. The contours indicate that the zone at which the NEPCM core undergoes solidification, which corresponds to the isotherm of T_{fu}, moves away from the cold inner tube as the fluid filling the cavity is cooling down.

has been heated to a maximum temperature, and a heat transfer takes place by free convection has halted. During this variation, in the period between the initial point and the steady zone, it can be seen that Nu_a is somewhat greater in the case of $\phi = 0.05$ compared to the other values. On the other side, Q increases from zero until stabilizing at its maximum value and is always higher for $\phi = 0.05$. Utilizing a greater concentration of NEPCM particles means that more particles undergo phase change and increases a contribution of NEPCM to a total transfer of heat occurring inside a cavity. It consequently raises the values of Nu_a and Q.

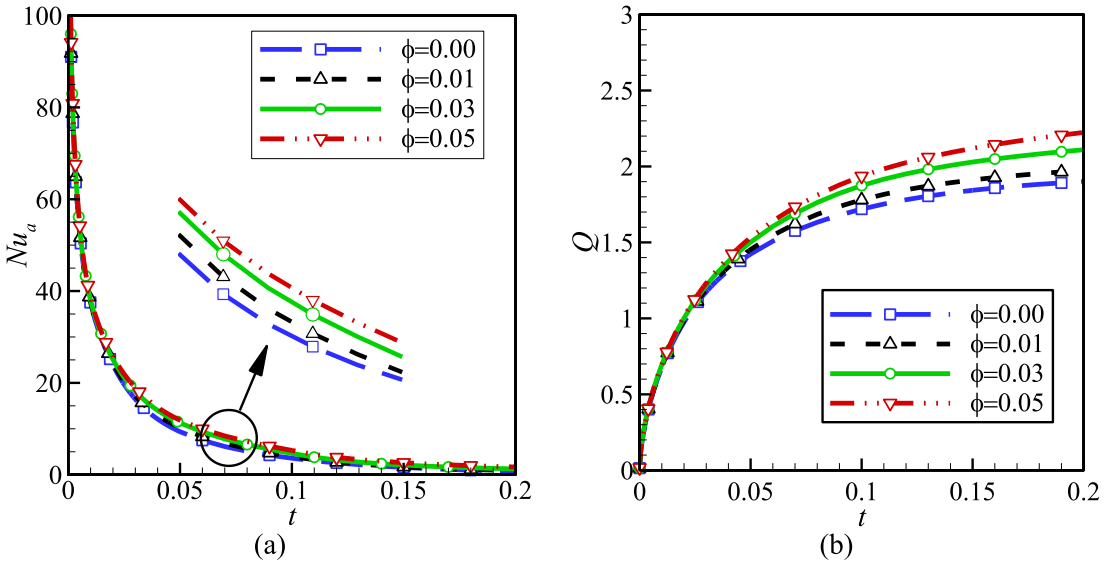

Fig. 14. The impact of different concentrations of the NEPCM particles on (a) Nusselt number (Nu_a) (b) Q during non-dimensional time when λ = 0.3225, Ste = 0.2, T_{fu} = 0.1, Da = 3.41 × 10^{-4} and Ra = 10^6. It can be seen that during the discharging state, both Nu_a and Q slightly increase with ϕ and are maximum for ϕ = 0.05. This is due to the augmented contribution of the NEPCM particles to the heat transfer for a high concentration of nanoparticles.

The isotherms, the contours of Cr_b, and the streamlines in the cavity at the same instant are shown in Fig. 9 for various quantities of T_{fu}. Here, the value of 0.97 shows the magnitude of Cr_b out of the phase transition zone. As phase transition take place this value rises. It can be seen that T_{fu} has a slight impact on the structure of flow patterns inside the cavity. Increasing T_{fu} shifts the low-temperature isotherms away from the inner heater and raises the overall temperature of the fluid in the cavity. The contours of Cr_b show that the zone at which the core of the NEPCM particles undergoes melting varies according to the corresponding isotherm. At t = 0.01, this zone is maximum for T_{fu} = 0.05, when the discrepancy between the inner tube temperature and fusion temperature is at its highest, while it remains limited to a small zone surrounding the inner heater tube when T_{fu} = 1, which is related to the observations discussed in Fig. 9.

To assess the impact of T_{fu} on thermal behavior, the variations of Nu_a and Q as functions of time are shown in Fig. 10 for different quantities of T_{fu}. Nu_a shows the same style of deviation for all the values of T_{fu}, while being slightly lower for T_{fu} = 1. The highest value of Nu_a slightly fluctuates between different values of T_{fu}, while Nu_a is always minimum for T_{fu} = 1 compared to the other values. A similar tendency can be seen for Q, which is always a minimum for T_{fu} = 1, while it is slightly higher for T_{fu} = 0.05 compared to the other values. Indeed, the NEPCM core undergoes a melting process once the surrounding temperature is near to T_{fu}. While T_{fu} = 1, the phase change occurs only in the small region surrounding the inner hot wall. In fact, reducing T_{fu} indicates that the larger part of a liquid is next to a temperature higher than T_{fu}, as can be observed in the isotherms of Fig. 7. So, the melting zone increases in size, and more particles pass the melting zone and experience phase change.

Fig. 11 shows the impact of Stefan number, i.e., Ste, upon the variations of Nu_a and Q as functions of time. It is shown that Nu_a and Q increase when Ste is reduced. This is because a latent heat of a core of a nano-additive rises when Ste is decreased, and the total transfer of heat is improved. The variations of Nu_a & Q as functions of time intended for different values of Rayleigh number are depicted in Fig. 12. Initially, raising Ra tends to increase Nu_a, and as time passes, the impact of the Ra becomes less important when the local temperature has reached its maximum. Similarly, Q rises with the usage of greater value of Ra. In fact, Ra remains as an indicator of the relative importance of the buoyancy forces driving the convective flow concerning the resistive viscous forces. Increasing Ra tends thus to increase the convective effects and improve heat transfer, translated by the increase of Q. Nonetheless, in the steady part, when all the fluid has reached the maximal temperature, the convection is diminished, and the effect of Ra becomes less important.

4.2. Solidification result (discharging state)

In this case, the temperature of an inner wall stays lower compared to a fusion temperature of a NEPCM core, which undergoes solidification. The discharging state is hence considered. The development of the isotherms, the contours of Cr_b, and the streamlines with time inside the cavity are illustrated in Fig. 13. At t = 0, the cold tube cools down its adjacent hot fluid. The temperature variance among a cold fluid & a hotter one filling a cavity initiates the convective flow. The temperature of the fluid keeps decreasing progressively until the whole fluid reaches a uniform low temperature. Subsequently, the strength of a convective stream grows at a beginning near the inner tube, and then, in the upper left part of the cavity, before gradually diminishing when the fluid temperature becomes uniform. The Cr_b contours indicate that the zone at which the NEPCM core undergoes solidification, which corresponds to the isotherm of T_{fu}, moves away from the cold inner tube as the fluid filling the cavity is cooling down.

The variations of Nu_a and Q as functions of time for various amount of ϕ is shown in Fig. 14. During the discharging state, both Nu_a and Q slightly increase with ϕ and are maximum for ϕ = 0.05. This is due to the augmented input of NEPCM particles to a transfer of heat when their volume fraction is increased.

Fig. 15 demonstrates the contours of Cr_b, the isotherms, and the streamlines in the cavity for various values of T_{fu} at t = 0.01. It is shown that the high-temperature isotherms are shifted downwards as T_{fu} is increased and, as a consequence, the portion of hot fluid is larger for higher T_{fu}. The core solidification zone also moves away from the inner tube following the evolution of the isotherm corresponding to T_{fu}, and a greater region of phase transformation thus emerges when T_{fu} increases. For T_{fu} = 0.05, a phase transformation zone is restricted close to an inner cold tube. In

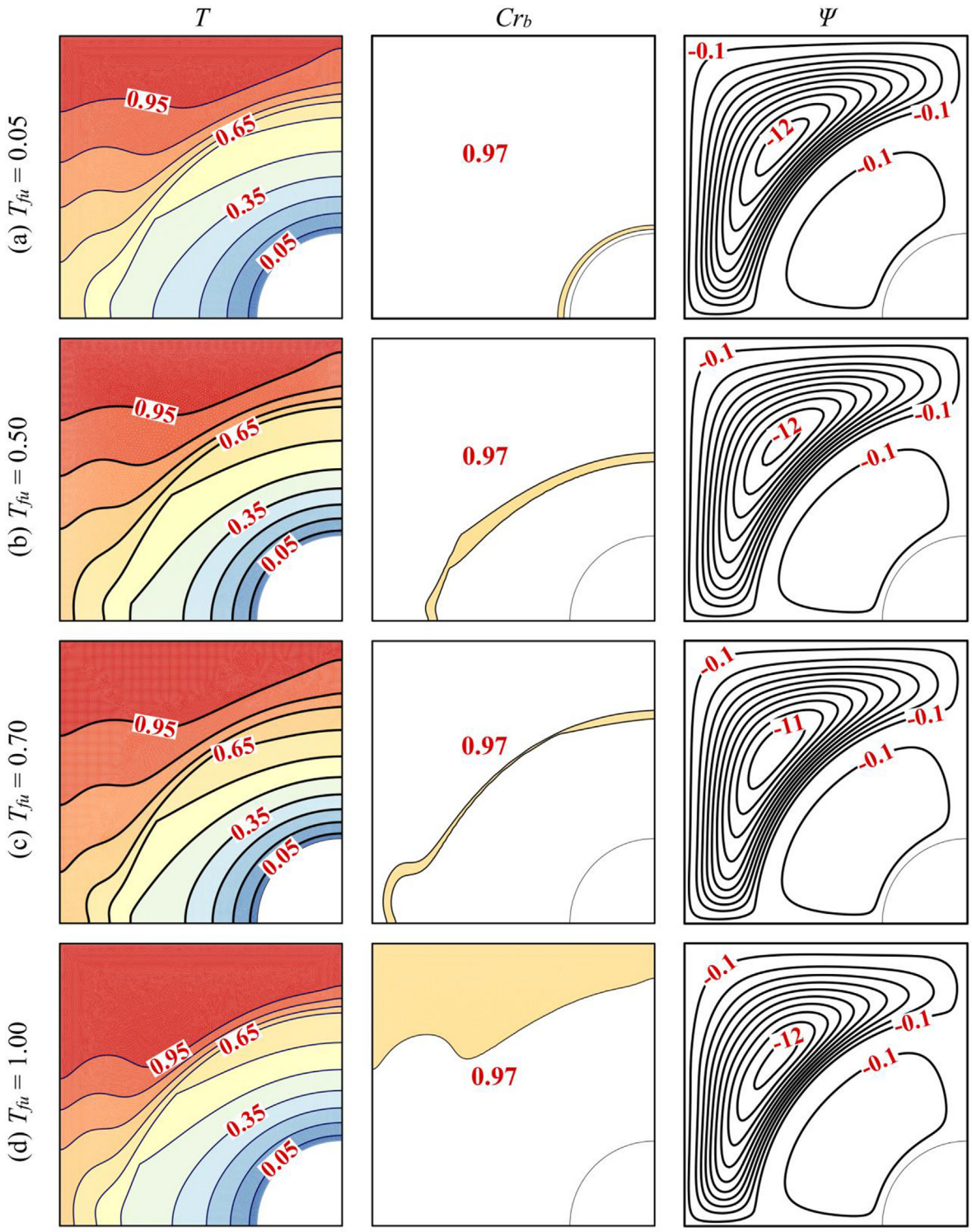

Fig. 15. The isotherm contours, Heat capacity ratio and Streamlines for four non-dimensional fusion temperatures of (a) T_{fu} = 0.05, (b) T_{fu} = 0.15, (c) T_{fu} = 0.30 and (d) T_{fu} = 1.00 in specific time t = 0.01 when λ = 0.3225, ϕ = 0.05, Ste = 0.2, Da = 3.41 × 10^{-4} and Ra = 10^6. It is shown that the high-temperature isotherms are shifted downwards as T_{fu} is increased, and the portion of hot fluid is larger for higher T_{fu}. The core solidification zone also moves away from the inner tube following the evolution of the isotherm corresponding to T_{fu}, and a greater region of phase transformation thus occurs when T_{fu} increases. For T_{fu} = 0.05, the phase transformation zone is restricted close to the cold inner tube. In addition, it is shown that the flow patterns remain almost unchanged for all the values of T_{fu}.

addition, it is shown that the flow patterns remain almost unchanged for all the values of T_{fu}.

Fig. 16 depicts the effect of T_{fu} on the variations of Nu_a and Q as functions of time. Nu_a is initially lower for T_{fu} = 0.05 compared to the other values; then, as time goes, it becomes maximum for this value of T_{fu}. Q is highest once a fusion temperature occurs between 0.5 and 0.7, whereas its minimum occurs for T_{fu} = 0.05. This variation is related to the development of the isotherms in the cavity, as observed in Fig. 13. The phase transformation of a NEPCM core by solidification takes place once the temperature of the surrounding

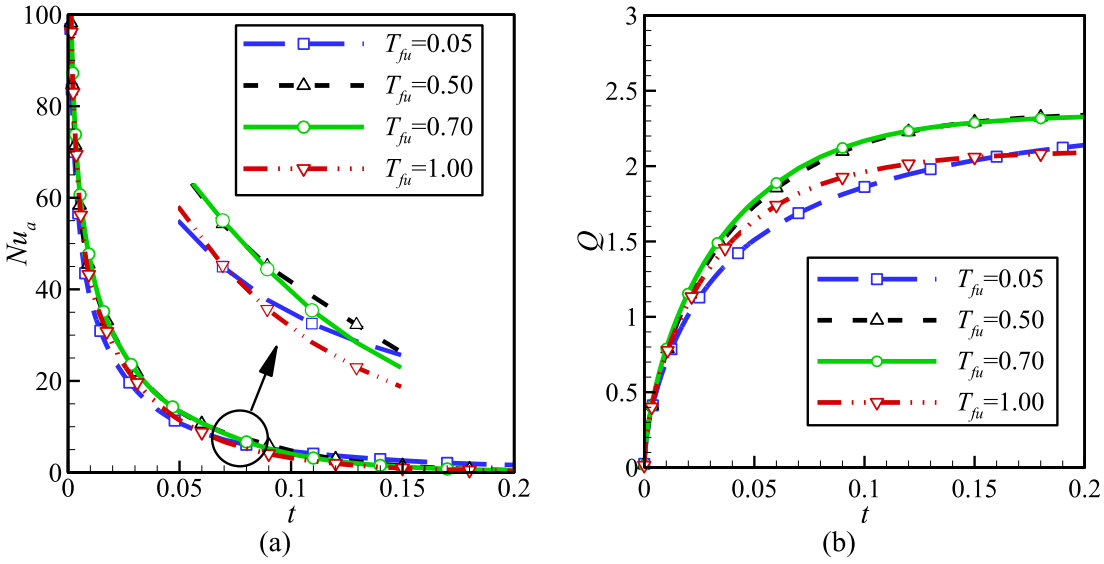

Fig. 16. The impact of different values of non-dimensional fusion temperature T_{fu} on (a) Nusselt number (Nu_a) (b) Q during non-dimensional time when λ = 0.3225, Ste = 0.2, ϕ = 0.05, Da = 3.41 × 10^{-4} and Ra = 10^6. Nu_a is initially lower for T_{fu} = 0.05 compared to the other values; then, as time goes, it becomes maximum for this value of T_{fu}. Q is highest when the fusion temperature is between 0.5 and 0.7, while its minimum occurs for T_{fu} = 0.05.

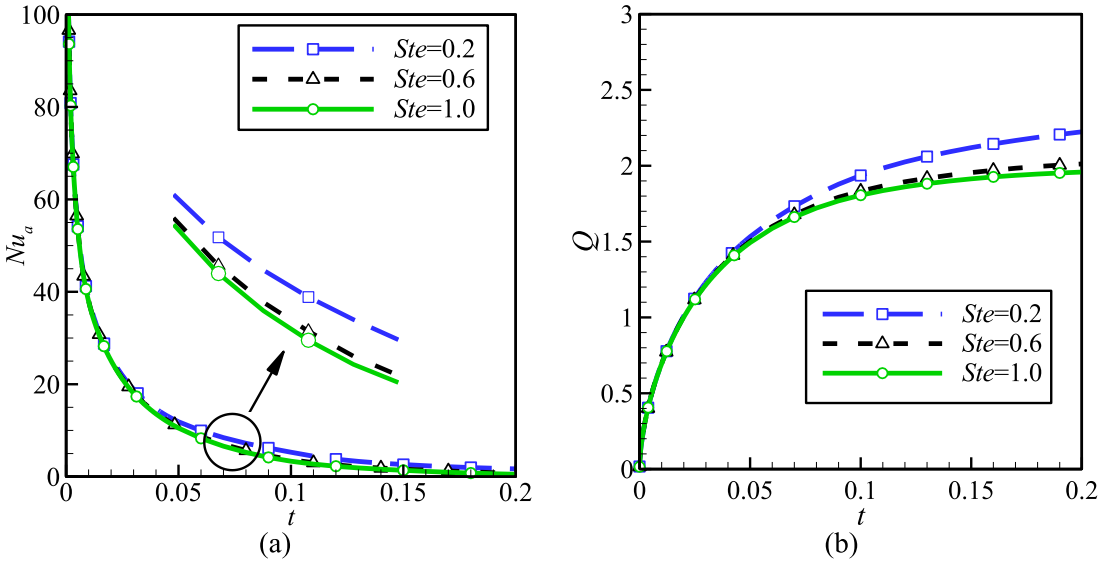

Fig. 17. The impact of different values of Ste number on (a) Nusselt number (Nu_a) (b) Q throughout non-dimensional time when λ = 0.3225, T_{fu} = 0.1, ϕ = 0.05, Da = 3.41 × 10^{-4} and Ra = 10^6. when Ste is decreased, Nu_a and Q increase.

is nearby T_{fu}. For T_{fu} = 0.05, this happens initially near the cold inner wall then progressively away from it. If T_{fu} is increased, the isotherm corresponding to T_{fu} is larger in size, and the phase change zone grows consequently. The particles, passing through that zone, experience phase change, thus enhancing heat transfer. When T_{fu} = 1, the phase change occurs in the region constricted near the outer walls, leading to a constraint in the transfer of heat compared to other values for T_{fu}.

The variations of Nu_a and Q as characteristics of time for different values of Ste have been plotted in Fig. 17. Both Nu_a and Q increase when Ste is decreased and are maximum for Ste = 0.2. The drop of Ste from 0.6 to 0.2 rises the ultimate stored energy (Q) about 25% at t = 0.2. This is due, as previously discussed, to the fact that the latent heat of the particle's core increases when Ste drops. The effect of Ra on the variations of Nu_a and Q as functions of time is illustrated in Fig. 18. As Ra growth the Nu_a mainly increases at the early stages of heat transfer, before the steady part of the curve where the effect of increasing Ra diminishes. On the other side, Q increases with Ra and is maximum for Ra = 10^6, due to the rise of the relative importance of the driving buoyancy forces concerning the viscous forces, promoting thus the convective heat transfer.

5. Conclusions

The energy storage and thermal nature of the NEPCM-suspension were studied into an enclosure. The phase change heat transfer of nanoparticles was taken into account using a temperature-dependent heat capacity function. The heat transfer rate and total stored energy were investigated for various fusion temperatures, Stefan numbers, Volume fractions, & Rayleigh numbers of nanoparticles. The temperature distribution patterns, phase change interface, and streamlines were also investigated. The key

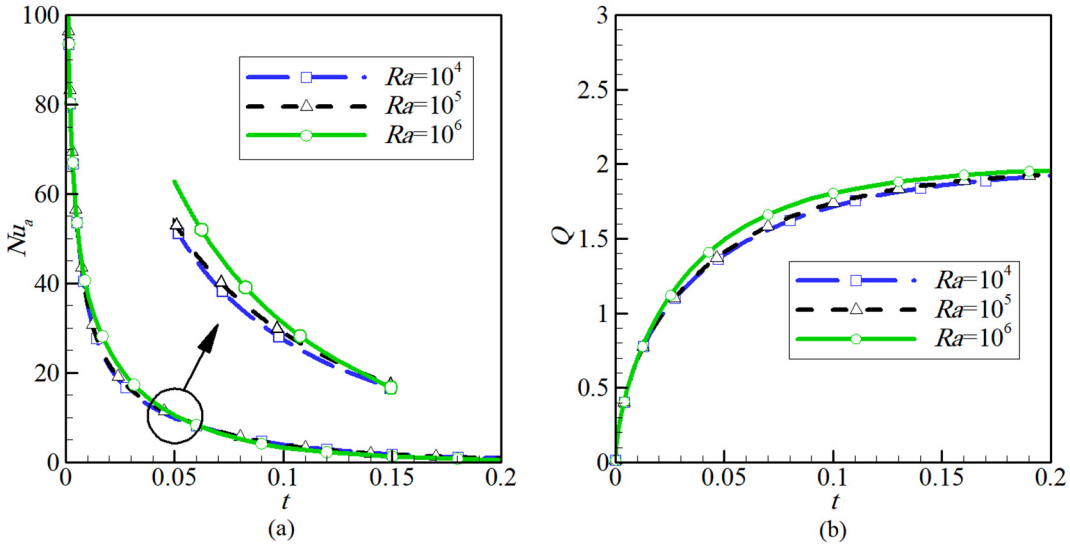

Fig. 18. The impact of different values of *Ra* number on (a) Nusselt number (Nu_a) (b) *Q* during non-dimensional time when λ = 0.3225, *Ste* = 0.2, T_{fu} = 0.1, ϕ = 0.05 and *Da* = 3.41 $\times$ 10^{-4}. When *Ra* increases Nu_a mainly in the first period of time, before the steady part of the curve where the effect of increasing *Ra* diminishes.

outcomes of current numerical research can be reported in the following way:

- Increasing the volume fraction ϕ enhances heat transfer and raises the amount of energy *Q* transferred from and into the active wall throughout the processes of charging & discharging, due to the intensified involvement of these particles to the overall transfer of heat inside the cavity. The transferred energy stays maximum when the NEPCM's 5% volume fraction is utilized.
- Raising Stefan number lessens the latent heat of the core of the particles. This consequently inhibits heat transfer and reduces *Q* during both melting and solidification by diminishing the involvement of particles in the overall heat transfer.
- Using a higher value of *Ra* increases the importance of the buoyancy forces driving the flow concerning the resistive viscous forces and, as a consequence, enhances heat transfer and raises the value of *Q*. Nonetheless, the effect of *Ra* is diminished in the steady regime when all the fluid in the cavity has been heated up or cooled down in the processes of charging & discharging correspondingly.
- An impact of a fusion temperature T_{fu} of the NEPCM cores on the transfer of heat & on *Q* closely follows the development of the isothermal contours and is different between the processes of charging & discharging, as the phase transformation occurs once the temperature of the surrounding is nearby T_{fu}. The transferred energy is minimal for T_{fu} = 1 and T_{fu} = 0.05 during the charging and discharging processes, respectively.

Declaration of Competing Interest

The authors declare that they have no known competing financial interests or personal relationships that could have appeared to influence the work reported in this paper.

Acknowledgments

Abdelraheem M. Aly extends his appreciation the Deanship of Scientific Research at King Khalid University, Abha, Saudi Arabia, for funding this work through the Research Group Project under Grant Number (RGP. 2/17/42).

References

[1] European Commission, European Union Energy in Figures; Statistical Pocketbook; Publications Office of the EU: Luxembourg, Luxembourg, 2016.
[2] S. Paltsev, Projecting Energy and Climate for the 21st Century, Econ. Energy Environ. Policy 9 (2020).
[3] J. Thomas, Drive cycle powertrain efficiencies and trends derived from EPA vehicle dynamometer results, SAE Int. J. Passenger Cars-Mech. Syst. 7 (2014) 1374–1384.
[4] L.O. Valøen, M.I. Shoesmith, The effect of PHEV and HEV duty cycles on battery and battery pack performance, in: Plug-in hybrid electric Vehicle Conference, 2007.
[5] P.T. Sardari, D. Giddings, D. Grant, M. Gillott, G.S. Walker, Discharge of a composite metal foam/phase change material to air heat exchanger for a domestic thermal storage unit, Renew. Energy 148 (2020) 987–1001.
[6] G.F. Frate, L. Ferrari, U. Desideri, Multi-criteria investigation of a pumped thermal electricity storage (PTES) system with thermal integration and sensible heat storage, Energy Convers. Manage. 208 (2020) 112530.
[7] G. Murali, K.R.K. Reddy, M.T.S. Kumar, J. SaiManikanta, V.N.K. Reddy, Performance of solar aluminium can air heater using sensible heat storage, Mater. Today:. Proc. 21 (2020) 169–174.
[8] A. Shahsavar, J. Khosravi, H.I. Mohammed, P. Talebizadehsardari, Performance evaluation of melting/solidification mechanism in a variable wave-length wavy channel double-tube latent heat storage system, J. Storage Mater. 27 (2020) 101063.
[9] M. Telkes, E. Raymond, Storing solar heat in chemicals—a report on the Dover house, Heat Vent 46 (11) (1949) 80–86.
[10] A. Arshad, M. Jabbal, P.T. Sardari, M.A. Bashir, H. Faraji, Y. Yan, Transient simulation of finned heat sinks embedded with PCM for electronics cooling, Therm. Sci. Eng. Progress (2020) 100520.
[11] A. Shahsavar, A. Goodarzi, H.I. Mohammed, A. Shirneshan, P. Talebizadehsardari, Thermal performance evaluation of non-uniform fin array in a finned double-pipe latent heat storage system, Energy 193 (2020) 116800.
[12] R. Velraj, R. Seeniraj, B. Hafner, C. Faber, K. Schwarzer, Experimental analysis and numerical modelling of inward solidification on a finned vertical tube for a latent heat storage unit, Sol. Energy 60 (1997) 281–290.
[13] P.T. Sardari, R. Babaei-Mahani, D. Giddings, S. Yasseri, M. Moghimi, H. Bahai, Energy recovery from domestic radiators using a compact composite metal Foam/PCM latent heat storage, J. Cleaner Prod. 257 (2020) 120504.
[14] J.M. Mahdi, H.I. Mohammed, E.T. Hashim, P. Talebizadehsardari, E.C. Nsofor, Solidification enhancement with multiple PCMs, cascaded metal foam and nanoparticles in the shell-and-tube energy storage system, Appl. Energy 257 (2020) 113993.
[15] X. Tang, W. Li, X. Zhang, H. Shi, Fabrication and characterization of microencapsulated phase change material with low supercooling for thermal energy storage, Energy 68 (2014) 160–166.
[16] Y. Yamagishi, T. Sugeno, T. Ishige, H. Takeuchi, A.T. Pyatenko, An evaluation of microencapsulated PCM for use in cold energy transportation medium, in: IECEC 96. Proceedings of the 31st Intersociety Energy Conversion Engineering Conference, IEEE, 1996, pp. 2077-2083.
[17] T. Toppi, L. Mazzarella, Gypsum based composite materials with micro-encapsulated PCM: Experimental correlations for thermal properties estimation on the basis of the composition, Energy Build. 57 (2013) 227–236.

[18] A. El Ouali, T. El Rhafiki, T. Kousksou, A. Allouhi, M. Mahdaoui, A. Jamil, Y. Zeraouli, Heat transfer within mortar containing micro-encapsulated PCM: Numerical approach, Constr. Build. Mater. 210 (2019) 422–433.
[19] E. Alehosseini, S.M. Jafari, Micro/nano-encapsulated phase change materials (PCMs) as emerging materials for the food industry, Trends Food Sci. Technol. (2019).
[20] Y. Wang, Z. Chen, X. Ling, A molecular dynamics study of nano-encapsulated phase change material slurry, Appl. Therm. Eng. 98 (2016) 835–840.
[21] J. Shi, X. Wu, R. Sun, B. Ban, J. Li, J. Chen, Nano-encapsulated phase change materials prepared by one-step interfacial polymerization for thermal energy storage, Mater. Chem. Phys. 231 (2019) 244–251.
[22] R. Heydarian, M.B. Shafii, A.R. Shirin-Abadi, R. Ghasempour, M.A. Nazari, Experimental investigation of paraffin nano-encapsulated phase change material on heat transfer enhancement of pulsating heat pipe, J. Therm. Anal. Calorim. 137 (2019) 1603–1613.
[23] T.E. Alam, Experimental investigation of encapsulated phase change materials for thermal energy storage, 2015.
[24] B. Kanimozhi, K. Harish, B.S. Tarun, P.S.S. Reddy, P.S. Sujeeth, Charging and Discharging Processes of Thermal Energy Storage System Using Phase change materials, in: IOP Conference Series: Materials Science and Engineering, IOP Publishing, 2017, pp. 012040.
[25] S. Bellan, J. Gonzalez-Aguilar, M. Romero, M.M. Rahman, D.Y. Goswami, E.K. Stefanakos, D. Couling, Numerical analysis of charging and discharging performance of a thermal energy storage system with encapsulated phase change material, Appl. Therm. Eng. 71 (2014) 481–500.
[26] M. Ghalambaz, S. Mehryan, I. Zahmatkesh, A. Chamkha, Free convection heat transfer analysis of a suspension of nano–encapsulated phase change materials (NEPCMs) in an inclined porous cavity, Int. J. Therm. Sci. 157 (2020) 106503.
[27] M. Ghalambaz, S. Mehryan, M. Mozaffari, S.M.H. Zadeh, M.S. Pour, Study of thermal and hydrodynamic characteristics of water-nano-encapsulated phase change particles suspension in an annulus of a porous eccentric horizontal cylinder, Int. J. Heat Mass Transf. 156 (2020) 119792.
[28] M. Ghalambaz, S.M.H. Zadeh, S. Mehryan, A. Haghparast, H. Zargartalebi, Free convection of a suspension containing nano-encapsulated phase change material in a porous cavity; local thermal non-equilibrium model, Heliyon 6 (2020) e03823.
[29] S. Mehryan, M. Ismael, M. Ghalambaz, Local thermal nonequilibrium conjugate natural convection of nano-encapsulated phase change particles in a partially porous enclosure, Math. Methods Appl. Sci. (2020).
[30] L. Chai, R. Shaukat, L. Wang, H.S. Wang, A review on heat transfer and hydrodynamic characteristics of nano/microencapsulated phase change slurry (N/MPCS) in mini/microchannel heat sinks, Appl. Therm. Eng. 135 (2018) 334–349.
[31] S. Barlak, O.N. Sara, A. Karaipekli, S. Yapıcı, Thermal conductivity and viscosity of nanofluids having nanoencapsulated phase change material, Nanoscale Microscale Thermophys. Eng. 20 (2016) 85–96.
[32] B. Chen, X. Wang, R. Zeng, Y. Zhang, X. Wang, J. Niu, Y. Li, H. Di, An experimental study of convective heat transfer with microencapsulated phase change material suspension: laminar flow in a circular tube under constant heat flux, Exp. Therm Fluid Sci. 32 (2008) 1638–1646.
[33] K. Khanafer, K. Vafai, A critical synthesis of thermophysical characteristics of nanofluids, Int. J. Heat Mass Transf. 54 (2011) 4410–4428.
[34] H.R. Seyf, Z. Zhou, H. Ma, Y. Zhang, Three dimensional numerical study of heat-transfer enhancement by nano-encapsulated phase change material slurry in microtube heat sinks with tangential impingement, Int. J. Heat Mass Transf. 56 (2013) 561–573.
[35] A. Biography, in: The Finite Element Method for Fluid Dynamics (Seventh Edition), Butterworth-Heinemann, Oxford, 2014, p. ii.
[36] K. Kahveci, Buoyancy driven heat transfer of nanofluids in a tilted enclosure, J. Heat Transfer 132 (2010) 062501.
[37] T.H. Kuehn, R.J. Goldstein, An experimental and theoretical study of natural convection in the annulus between horizontal concentric cylinders, J. Fluid Mech. 74 (1976) 695.
[38] G. Cesini, M. Paroncini, G. Cortella, M. Manzan, Natural convection from a horizontal cylinder in a rectangular cavity, Int. J. Heat Mass Transf. 42 (1999) 1801–1811.
[39] P. Nithiarasu, K. Seetharamu, T. Sundararajan, Natural convective heat transfer in a fluid saturated variable porosity medium, Int. J. Heat Mass Transf. 40 (1997) 3955–3967.